ELSEVIER

Contents lists available at ScienceDirect

Solid State Communications

journal homepage: www.elsevier.com/locate/ssc





Strain tuned low thermal conductivity in Indium Antimonide (InSb) through increase in anharmonic phonon scattering - A first-principles study

Rajmohan Muthaiah*, Fatema Tarannum, Jivtesh Garg

School of Aerospace and Mechanical Engineering, University of Oklahoma, Norman, OK, 73019, USA

ARTICLE INFO

Communicated by J. Fontcuberta

Keywords: Thermoelectric materials Biaxial compressive strain Indium Antimonide Thermal conductivity reduction

ABSTRACT

InSb is a promising thermoelectric material and a decrease in its thermal conductivity (k) can further improve its thermoelectric performance. Using first-principles computations, we report a 29% decrease in k of InSb through strain. k value decreases from 18.8 W/mK for unstrained InSb to 13.4 W/mK for 5% biaxially compressed InSb at 300 K. This decrease in k is found to be due to a large increase in anharmonic scattering of longitudinal acoustic (LA) phonons in strained InSb by almost 330% in Brillouin-zone center, driven by shift of transverse acoustic (TA) phonons to lower frequencies in strained InSb. This shift leads to a simultaneous increase in number of decay scattering channels and a two-fold increase in the magnitude of three-phonon coupling elements, leading to the observed large increase in scattering rates of LA phonons. Scattering of transverse acoustic (TA) phonons is also found to increase by \sim 61% at Brillouin-zone edge, facilitated by an increase in number of absorption scattering channels. First-principles computations based on deriving interatomic force interactions from density-functional theory are used to provide detailed understanding of increase in phonon scattering rates in strained InSb.

1. Introduction

Indium Antimonide (InSb) is a promising candidate material for thermoelectric applications [1-3] because of its high mobility of electrons of about 10^4 – 10^5 cm²V⁻¹s⁻¹ and bandgap of about 0.18 eV [4]. The performance of a thermoelectric material can be expressed by the dimensionless figure of merit, $ZT = \sigma S^2 T/k$, where σ , S, T and k are the electrical conductivity, Seebeck coefficient, absolute temperature and thermal conductivity respectively. Thermoelectric performance of InSb can be increased by increasing the power factor (σS^2) [5,6] and reducing lattice thermal conductivity [7,8]. Various strategies such as disorder [9, 10], nano structuring [11,12], strain [13] and defects [14,15] can be used to reduce the lattice thermal conductivity. In this letter, we report 29% and 17% reduction in in-plane (plane in which compressive biaxial strain is applied) and out-of-plane thermal conductivity of cubic InSb through 5% biaxial compressive strain. This decrease in *k* is found to be due to a large increase in three-phonon scattering rates of LA phonons driven by a shift of TA frequencies to lower values. Simultaneously TA phonon scattering rates also increase mediated by an increase in absorption scattering channels in strained InSb. First-principles computations are used to present understanding of the role of strain in modifying scattering rates in strained InSb. These results have important implications for high efficiency thermoelectric materials.

2. Thermal conductivity computation

Thermal conductivity in this work is predicted for cubic Indium Antimonide using first principles approach [10,16-18] by exactly [16] solving the phonon Boltzmann transport equation (PBTE). The most important ingredients, namely the 2nd and 3rd order interatomic force constants (IFCs), needed for k prediction, are derived from density-functional perturbation theory (DFPT) [19,20]. DFT has been shown to yield highly accurate IFCs, overcoming limitations of empirical potentials, leading to unprecedented accuracy [18] in the prediction of lattice k for defect free materials. For analysis, it is useful to look at the expression for thermal conductivity (k) prediction, based on solving PBTE [10] in the single mode relaxation time (SMRT) approximation, given by Ref. [21],

$$k_{\alpha} = \frac{\hbar^2}{N\Omega k_b T^2} \sum_{\lambda} v_{a\lambda}^2 \omega_{\lambda}^2 \overline{n}_{\lambda} \left(\overline{n}_{\lambda} + 1 \right) \tau_{\lambda} \tag{1}$$

where $\alpha, \hbar, \Omega, k_b$, T, are the cartesian direction, Planck constant, unit cell

E-mail address: rajumenr@ou.edu (R. Muthaiah).

^{*} Corresponding author.

volume, Boltzmann constant, and absolute temperature respectively. λ represents the vibrational mode (qj) (q is the wave vector and j represents phonon polarization). N is the size of the q mesh used for summation in above equation. ω_{λ} , \overline{n}_{λ} , and $v_{\alpha\lambda}$ $(=\partial\omega_{\lambda}/\partial q)$ are the phonon frequency, equilibrium Bose-Einstein population and group velocity along cartesian direction α , respectively of a phonon mode λ . These are derived from the knowledge of phonon dispersion computed using 2nd order IFCs. τ_{λ} is the phonon lifetime (equal to the inverse of scattering rate). In the SMRT approximation, phonon lifetime (τ_{λ}) of a vibrational mode λ is computed using the following equation.

$$\begin{split} &\frac{1}{\tau_{\lambda}} = \pi \sum_{\lambda',\lambda''} \left| V_{3}(-\lambda,\lambda',\lambda'') \right|^{2} \times \left[2 \left(n_{\lambda'} - n_{\lambda''} \right) \delta \left(\omega(\lambda) + \omega(\lambda') - \omega(\lambda'') \right) \right. \\ &+ \left(1 + n_{\lambda'} + n_{\lambda''} \right) \delta \left(\omega(\lambda) - \omega(\lambda') - \omega(\lambda'') \right) \end{split} \tag{2}$$

where $V_3(-\lambda,\lambda',\lambda'')$ are the three-phonon coupling matrix elements computed using both 2nd and 3rd order IFCs. The first delta function in the above equation represents absorption scattering process, where a phonon mode $(q\omega)$ scatters by absorbing another phonon mode $(q'\omega')$, yielding a higher energy $(q''\omega'')$ phonon mode, and second delta function represents a decay process, where a phonon mode decays into two lower energy phonons. These processes satisfy energy and momentum conservation given by $\omega+\omega'=\omega''$ (energy), q+q'=q'' (momentum) for absorption process and $\omega=\omega'+\omega''$ (energy), q=q'+q'' (momentum) for decay process.

3. Results

Lattice parameter of unstrained InSb was determined through energy minimization to be $a_0=6.389$ Å. For the strained cases, the lattice was compressed by 5% in the x-y plane (along both x and y directions) and relaxed in the z-direction. The lattice dimensions of the biaxially strained InSb are computed to be $a=b=0.95a_0$, and c=1.108a.

Computed phonon dispersion for unstrained (which is in good agreement with the experimental measurements [24]) and strained case is shown in Fig. 1. Strain is found to shift TA phonon frequencies to lower values (seen also a shift in phonon density of states) while leading to an increase in LA phonon frequencies.

At 300 K, thermal conductivity of unstrained InSb is computed to be $18.83~{\rm Wm}^{-1}{\rm K}^{-1}$ (Fig. 2), in good agreement with measurements [24]. Upon biaxial compression, k is reduced to $13.38~{\rm Wm}^{-1}{\rm K}^{-1}$ and $15.62~{\rm Wm}^{-1}{\rm K}^{-1}$ along in-plane and out-of-plane directions, representing a reduction of 29% and 17%, respectively. To understand this reduction and anisotropy in k in strained InSb, we analyze the effect of strain on phonon group velocities and scattering rates in Fig. 3.

Fig. 3a shows large increase in scattering rates of acoustic phonons in strained InSb, particularly for the LA phonons. At a frequency of \sim 70 cm⁻¹, the scattering rate of LA phonon for example, increases by nearly a factor of 5 from \sim 0.5 cm⁻¹ to \sim 2.5 cm⁻¹, at 300 K. Scattering rates of TA phonons also increase in strained InSb, however, the increase is smaller than for LA phonons. Mean phonon velocities, along the in-plane direction (plane in which bi-axial strain is applied), however, are found to remain almost the same for unstrained and strained InSb (Fig. 3b). Decrease in in-plane k in strained InSb is, therefore, primarily due to an increase in scattering rates. Along the, out-of-plane direction, an

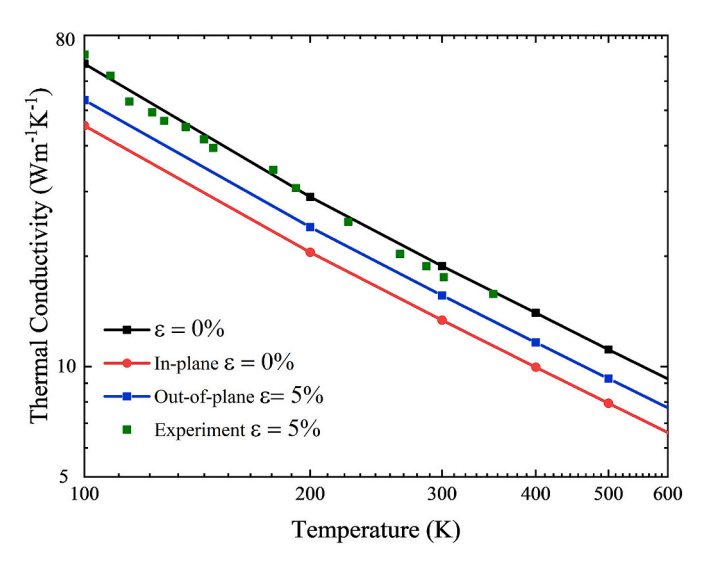


Fig. 2. Computed in-plane and out-of-plane thermal conductivity of unstrained and 5% biaxially compressed InSb.

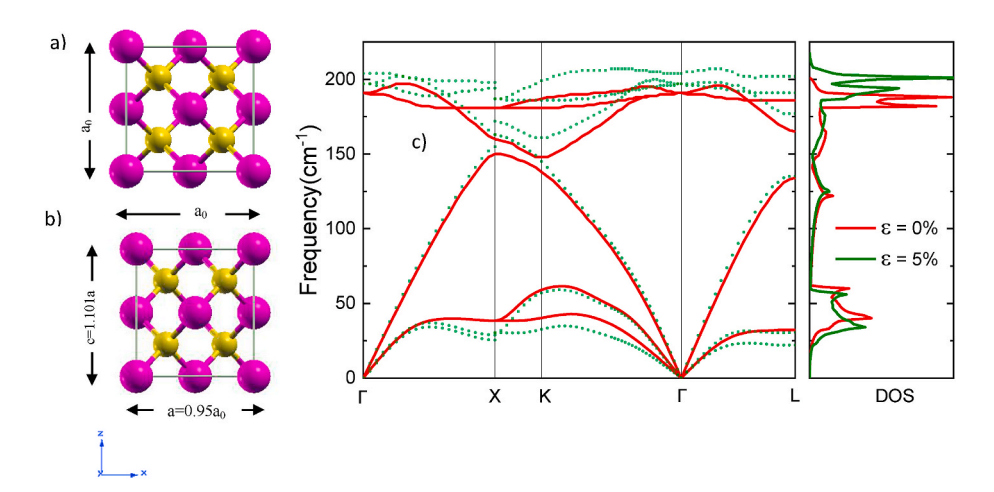


Fig. 1. Indium Antimonide with a)0% and b) 5% strain c) Phonon dispersion and density of state for unstrained and biaxial compressive strained InSb. Note: For the purpose of comparison, we plotted along the same direction.

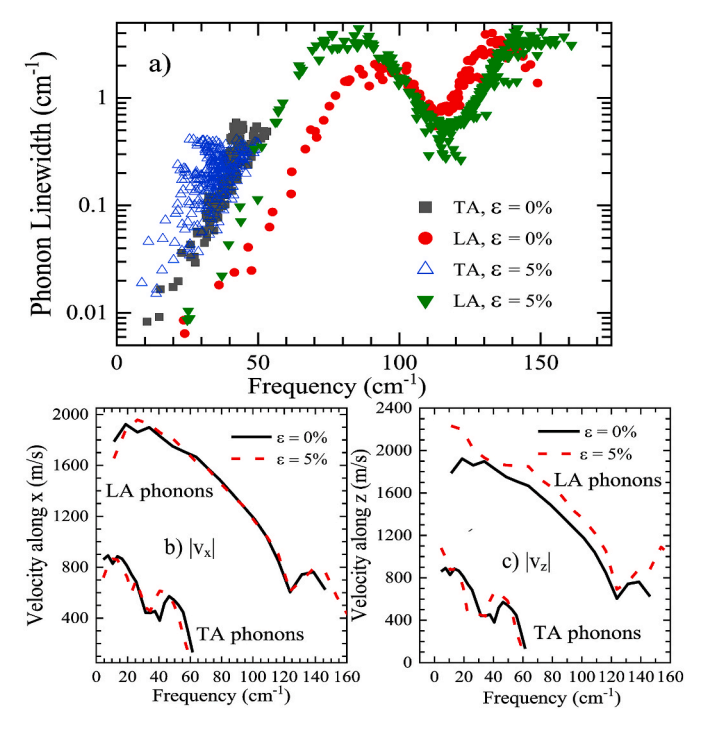


Fig. 3. Comparison between unstrained and strained InSb of a) Phonon linewidths at 300 K b) mean velocity in in-plane x-direction and c) mean velocity in out-of-plane z-direction. Note: We have plotted TA and LA phonons along different directions in supplementary information.

increase in phonon velocities of LA phonons in strained InSb (Fig. 3c), partially cancels the effect of increase in scattering rates, leading to lower decrease in k along this direction.

4. Increase in LA phonon scattering

To understand increase in phonon scattering in strained InSb, we analyze the scattering rates of LA and TA phonons along Γ -X in Fig. 4. A large increase of 330% in scattering rate of LA phonon is observed in

strained InSb at wavevectors close to the middle of the Brillouin zone (at $q_x=0.45$) in Fig. 4a. Fig. 4c shows that a dominant contribution to scattering of LA phonons is from the $a\rightarrow a+a$ channel which represents decay of an acoustic phonon into two lower frequency acoustic phonons. The scattering rate for the $a\rightarrow a+a$ channel is found to peak with respect to wavevector for unstrained InSb at $q_x=0.60$ (Fig. 4e); in strained InSb, the scattering rate for this channel increases at lower wave-vectors, seen also as a shift in peak scattering rate to lower wavevector of $q_x=0.45$. The peak scattering rate for $a\rightarrow a+a$ channel for LA phonons increases significantly in magnitude in strained InSb, by almost a factor of 2 relative to peak in unstrained InSb (Fig. 4e).

Fig. 1 shows that strain shifts TA phonons to lower frequencies. Above increase in scattering rate of mid-Brillouin zone LA phonons is found to be due to this decrease in TA frequencies, through two important effects – a) an increase in number of decay scattering channels and b) an increase in magnitude of three-phonon coupling elements, as described next. We first describe increase in number of decay channels for LA phonons at mid-Brillouin zone wave-vectors. To understand this increase, it is realized that scattering rate of $a_{LA} \rightarrow a + a$ channel is almost entirely due to decay of LA phonons in to two TA phonons, i.e the $a_{LA} \rightarrow a_{TA} + a_{TA}$ channel, as seen in Fig. 4e. Decrease in TA phonon frequencies in strained InSb (Fig. 1), increases the probability of scattering of lower frequency LA phonons in to these larger number of TA phonons now available at lower frequencies, leading to an increase in number of $a_{LA} \rightarrow a_{TA} + a_{TA}$ scattering (decay) channels, for low frequency (mid Brillouin zone) LA phonons in strained InSb.

To show this increase clearly, we define scattering phase space Φ for the $a_{LA} \rightarrow a_{TA} + a_{TA}$, as $\Phi = 1/(4N) \sum_{j'} \delta(\omega_{LA}({\pmb q}) - \omega_{TA}({\pmb q}') - \omega_{TA}({\pmb q}'' = {\pmb q} - {\pmb q})$

q'), N is the size of the q' mesh used for summation (summation is performed only over the TA modes). The phase space as defined above, is indicative of the number of decay scattering channels contributing to the magnitude of $a_{LA} \rightarrow a_{TA} + a_{TA}$ channel (the definition essentially assumes all of the three-phonon coupling elements to be unity, and ignores absorption processes in Equation (2)). Fig. 5a shows an increase in scattering phase space for LA phonons at smaller wavevectors (lower frequencies) in strained InSb (Fig. 5a). While peak phase space for unstrained InSb occurs at $q_x \sim 0.60$, this peak shifts to lower wavevector of

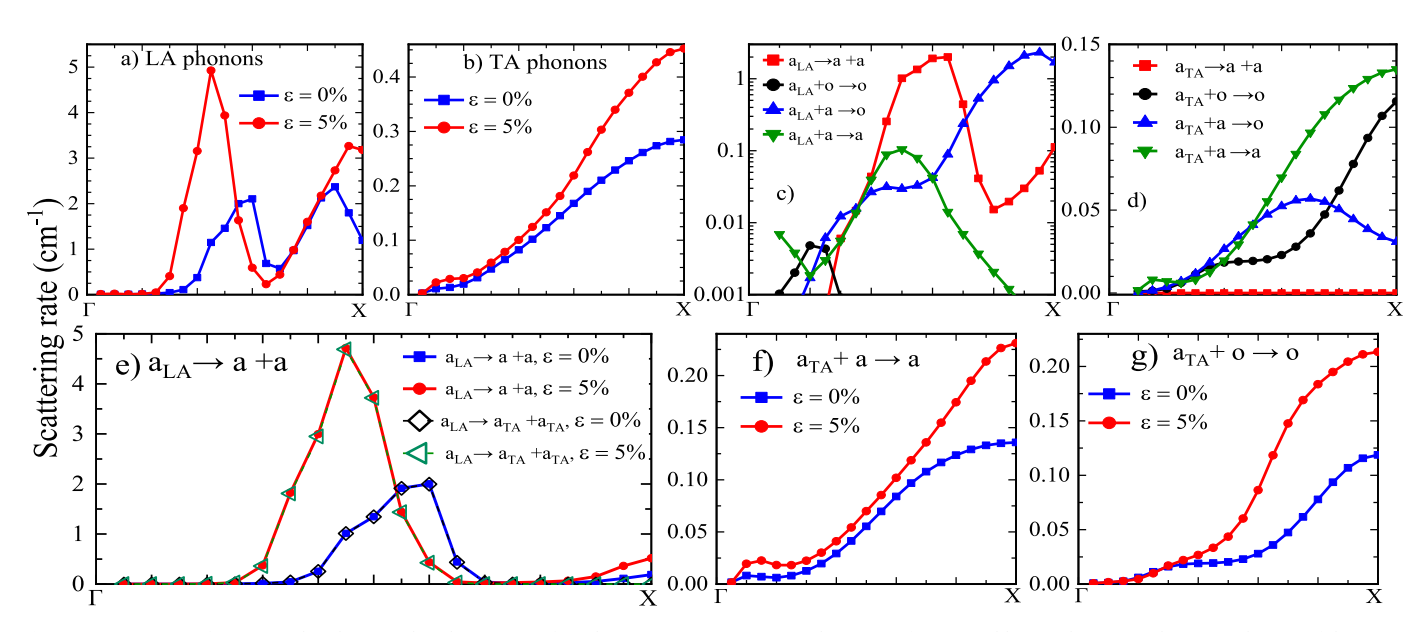


Fig. 4. Comparison of unstrained and strained InSb in terms of total scattering rate at 300 K along Γ -X of a) LA and b) TA phonon modes. Contribution of dominant scattering channels at 300 K in unstrained InSb for c) LA and d) TA phonons. Comparison between unstrained and strained InSb of e) aLA \rightarrow a+a channel, f) aTA+a \rightarrow a channel and g) aTA + o \rightarrow o channel at 300 K. **Note:** Since, magnitude of LA scattering varies from 0.001 to 3, we used the logarithmic scale for clear visualization in Fig. 4c.

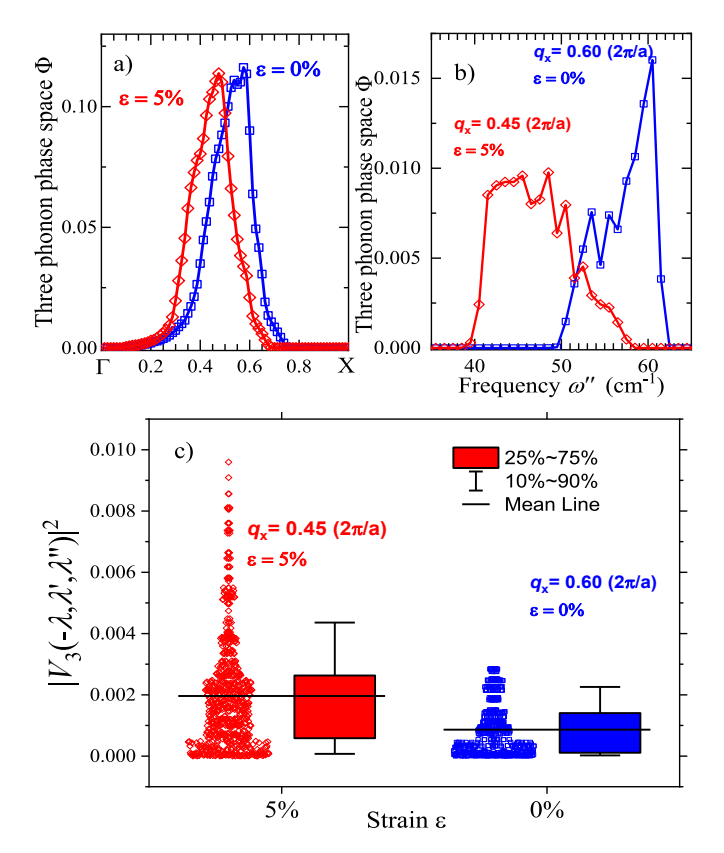


Fig. 5. a) Phase space for scattering of LA phonons in strained and unstrained InSb b) phase space for scattering of LA at different frequencies and c) Comparison of three-phonon coupling elements in strained and unstrained InSb.

 $q_x\sim$ 0.45 in strained InSb. At wavevector $q_x=0.45$, phase space for scattering of LA phonon in strained InSb is almost 55% higher, relative to the case of unstrained InSb (Fig. 5a).

To see that this increase in phase space for lower frequency LA phonons is directly due to shift of TA frequencies to lower values, we show distribution of TA phonon frequencies contributing to the scattering phase space for $a_{LA} \rightarrow a_{TA} + a_{TA}$ channel in Fig. 5b. This distribution is shown as a function of the larger of the two TA phonon frequencies involved in decay of LA phonon through $\omega_{LA} = \omega_{TA}' + \omega_{TA}''$, denoting it by ω'' on x-axis in Fig. 5b. This split of overall phase space for the channel $a_{LA} \rightarrow a_{TA} + a_{TA}$ into contributing frequencies is shown at the two wavevectors discussed above, namely, $q_x = 0.60$ for unstrained and $q_x = 0.45$ for strained cases (wavevectors at which $a_{LA} \rightarrow a + a$ channel is seen to peak in Fig. 4e) and Fig. 5b shows that the peak contribution to scattering of LA phonon at $q_x = 0.60$ ($\omega = 103$ cm $^{-1}$) in unstrained InSb is from TA phonons with frequency $\omega'' \sim 60 \text{ cm}^{-1}$ (with corresponding $\omega'=43 \text{ cm}^{-1}$); these frequencies correspond to the two peaks in phonon density of states (Fig. 1). In strained InSb, however, Fig. 5b shows that strong contribution to scattering of LA phonon at $q_x = 0.45$ ($\omega = 82.2$ cm⁻¹) is from TA phonons of much lower frequencies, with peak contribution occurring from $\omega'' \sim 48 \text{ cm}^{-1}$ (with $\omega' = 34.2 \text{ cm}^{-1}$) (Fig. 5b) in strained InSb. This provides evidence of the dominant role of lower frequency TA phonons in increasing scattering rates of mid-Brillouin zone LA phonons in strained InSb.

However, while the peak phase space shifts to lower wavevector in strained InSb relative to unstrained InSb, the peak value of this phase space remains almost the same in magnitude (\sim 0.11) for strained and unstrained cases (Fig. 5a), and cannot alone explain the \sim 2-fold higher peak scattering rate in strained InSb (seen in Fig. 4b), relative to peak rate for unstrained InSb. This increase can be explained by an increase in magnitude of three-phonon coupling elements in strained InSb. Notice that the three-phonon coupling elements $|V_3(-\lambda,\lambda',\lambda'')|^2$ in equation (2)

are inversely proportional to the product of the three frequencies involved in scattering [21], $|V_3(-\lambda,\lambda',\lambda'')|^2 \propto \frac{1}{\omega(\lambda)\omega'(\lambda')\omega''(\lambda')}$. A shift in scattering to lower frequencies in strained InSb increases the magnitude of these coupling elements. The approximate ratio of $|V_3(-\lambda,\lambda',\lambda'')|^2$ corresponding to peak frequency contributions to scattering of wavevector $q_x = 0.60$ in unstrained and $q_x = 0.45$ strained InSb (described above and shown in Fig. 5b) can be computed as $\frac{\left|V_3(-\lambda,\lambda^\prime,\lambda'')\right|_{strain.~qx=0.45}^2}{\left|V_3(-\lambda,\lambda^\prime,\lambda'')\right|_{unstrain.~qx=0.60}^2} =$ $\frac{(103)(43)(60)}{(82.2)(34.2)(48)} = 1.97$. Distribution of all $|V_3(-\lambda,\lambda',\lambda'')|^2$ involved in scattering of LA phonons at the two wavevectors is also shown in Fig. 5c. Overall, the average value of $|V_3(-\lambda, \lambda', \lambda'')|^2$ involved in scattering of LA phonon at $q_x = 0.45$ in strained InSb is found to be almost two-fold higher relative to the case of $q_x = 0.60$ in unstrained InSb. These higher magnitudes of three-phonon coupling elements (Fig. 5c) combined with increase in scattering phase space (Fig. 5a) lead to the observed large increase in scattering rates of LA phonons in the middle of the Brillouin zone in strained InSb.

5. Increase in TA phonon scattering

For TA modes, strain is found to increase the magnitude of $a + a \rightarrow a$ and $a + o \rightarrow o$ scattering channels (Fig. 4f and g, respectively) leading to an increase in TA phonon scattering rate by a maximum of ~60% close to zone edge (point X) (Fig. 4b). Increase in $a + a \rightarrow a$ scattering for TA phonons can be understood by an increase in frequencies of LA phonons in strained InSb. Fig. 1 shows that, while, maximum LA phonon frequency in unstrained InSb is 150.4 cm⁻¹, the peak frequency in strained InSb is 162.8 cm⁻¹. This increase in LA frequencies introduces new a + $a\rightarrow a$ channels for TA phonons. This is seen through an example, by considering that in strained InSb, a TA phonon of frequency ω =20 cm⁻¹ can scatter by absorbing an LA phonon of frequency $\omega'=140~{\rm cm}^{-1}$, yielding an LA phonon of frequency $\omega''=160 \text{ cm}^{-1}$, thus satisfying energy conservation $\omega + \omega' = \omega''$ (provided the momentum conservation is satisfied) (Fig. 1). In unstrained case, however, LA phonon frequencies are lower, and an LA phonon of frequency $\omega''=160 \text{ cm}^{-1}$ does not exist, forbidding this channel. The presence of additional scattering channels in strained InSb leads to increase in $a + a \rightarrow a$ scattering for TA phonons. The effect is found to lead to larger increase in scattering at higher wavevectors (Fig. 4b and f); this can be understood by realizing that a TA phonon of frequency ω can only scatter into a final LA phonon of frequency ω'' higher than ω , restricting the frequency range $(\omega''_{LA, max} - \omega)$ for scattering as ω increases. Increase in LA frequencies in strained InSb by increasing this frequency range, thus resulting in a more dramatic increase in scattering of higher frequency TA phonons.

Increase in $a+o\rightarrow o$ channel for TA phonons can similarly be understood in terms of increase in optical frequency range in strained InSb. While in unstrained InSb, optical phonons range from 140.8 to 200.5 cm $^{-1}$, in strained InSb, the corresponding range is from 144.1 to 217.7 cm $^{-1}$. This increase in optical phonon frequency range introduces new channels for scattering of higher frequency TA phonons. This can be again be seen through an example, by considering that in strained InSb, a TA phonon of frequency 30 cm $^{-1}$ can absorb an optical phonon of frequency 180 cm $^{-1}$ to yield an optical phonon of frequency 210 cm $^{-1}$. However, in unstrained such a scattering channel is forbidden because of the lower optical phonon frequencies.

Above presented increase in scattering rates of TA and LA phonons diminishes their k contributions in strained InSb. While in unstrained InSb, TA and LA phonons contribute 10.52 and 8.30 W/mK to total k at 300 K, in strained InSb, their contribution decreases to 7.91 and 5.47 W/mK, respectively, along the in-plane direction, leading to the observed 29% decrease in k. Strain induced increase in phonon scattering may provide avenues to enhance thermoelectric efficiency through above

demonstrated decrease in k. Biaxial strain investigated in this work, can be achieved by growth of a material on a lattice mismatched substrate [25], providing avenues for realization of outlined decrease in k in applications.

6. Conclusion

In summary, using first principles approach we have provided a microscopic description of decrease in thermal conductivity (k) in strained Indium Antimonide (InSb). While k of unstrained InSb is computed to be 18.82 W/mK at 300 K, upon 5% biaxial compression, kdecreases to 13.38 W/mK and 15.62 W/mK along in-plane (plane in which biaxial strain is applied) and out-of-plane directions. This reduction in k is due to increase in phonon scattering rates of both longitudinal (LA) and transverse (TA) acoustic phonons. Increase in scattering of LA phonons is found to be due to a shift in TA phonon frequencies to lower values in strained InSb, which both increases the phase space for scattering and the magnitude of three-phonon coupling elements involved in scattering of mid-Brillouin zone LA phonons, leading to a large 330% increase in scattering rate of zone-center LA phonons. Increase in TA scattering rates is found to be due to increase in LA and optical phonon frequencies in strained InSb, which increase the number of absorption scattering channels for TA phonons. These results have important implications for design of high efficiency InSb based thermoelectrics.

Funding

The data that supports the findings of this study are available within the article. RM, FT and JG acknowledge financial support from National Science Foundation CAREER award under Award No. 1847129.

Author statements

Conceptualization- R.M and J.G. Data curation - R.M and F.T. Formal analysis – R.M, F.T and J.G. Funding acquisition – J.G. Investigation – R. M, F.T and J.G. Methodology – R.M and J.G. Project administration – R. M and J.G. Resources – J.G. Software- R.M and J.G. Supervision- J.G. Validation – F.T. Roles/Writing - original draft – R.M, F.T and J.G. Writing - review & editing – R.M, F.T and J.G.

Declaration of competing interest

The authors declare that they have no known competing financial

interests or personal relationships that could have appeared to influence the work reported in this paper.

Appendix A. Supplementary data

Supplementary data to this article can be found online at https://doi. org/10.1016/j.ssc.2021.114378.

References

- Y. Cheng, J. Yang, Q. Jiang, D. He, J. He, Y. Luo, D. Zhang, Z. Zhou, Y. Ren, J. Xin, J. Mater. Chem. 5 (10) (2017) 5163–5170.
- [2] K. Wang, P. Qin, Z.-H. Ge, J. Feng, Mater. Lett. 209 (2017) 373-375.
- [3] Z. Du, X. Chen, J. Zhu, J. Cui, Curr. Appl. Phys. 18 (8) (2018) 893–897.
- [4] D.L. Rode, Phys. Rev. B 3 (10) (1971) 3287-3299.
- [5] W. Liu, X. Tan, K. Yin, H. Liu, X. Tang, J. Shi, Q. Zhang, C. Uher, Phys. Rev. Lett. 108 (16) (2012) 166601.
- [6] Y. Pei, X. Shi, A. LaLonde, H. Wang, L. Chen, G.J. Snyder, Nature 473 (7345) (2011) 66–69.
- [7] K. Biswas, J. He, Q. Zhang, G. Wang, C. Uher, V.P. Dravid, M.G. Kanatzidis, Nat. Chem. 3 (2) (2011) 160–166.
- [8] B. Poudel, Q. Hao, Y. Ma, Y. Lan, A. Minnich, B. Yu, X. Yan, D. Wang, A. Muto, D. Vashaee, X. Chen, J. Liu, M.S. Dresselhaus, G. Chen, Z. Ren, Science 320 (5876) (2008) 634.
- [9] S. Mukherjee, U. Givan, S. Senz, M. de la Mata, J. Arbiol, O. Moutanabbir, Nano Lett. 18 (5) (2018) 3066–3075.
- [10] J. Garg, N. Bonini, B. Kozinsky, N. Marzari, Phys. Rev. Lett. 106 (4) (2011), 045901.
- [11] Y. Nakamura, Sci. Technol. Adv. Mater. 19 (1) (2018) 31-43.
- [12] S. Perumal, S. Roychowdhury, K. Biswas, Inorganic Chemistry Frontiers 3 (1) (2016) 125–132.
- [13] D.-S. Tang, G.-Z. Qin, M. Hu, B.-Y. Cao, J. Appl. Phys. 127 (3) (2020), 035102.
- [14] R. Stern, T. Wang, J. Carrete, N. Mingo, G.K.H. Madsen, Phys. Rev. B 97 (19) (2018) 195201.
- [15] G.-K. Ren, J.-L. Lan, K.J. Ventura, X. Tan, Y.-H. Lin, C.-W. Nan, npj Computational Materials 2 (1) (2016) 16023.
- [16] G. Fugallo, M. Lazzeri, L. Paulatto, F. Mauri, Phys. Rev. B 88 (4) (2013), 045430.
- [17] L. Paulatto, F. Mauri, M. Lazzeri, Phys. Rev. B 87 (21) (2013) 214303.
- [18] D.A. Broido, M. Malorny, G. Birner, N. Mingo, D.A. Stewart, Appl. Phys. Lett. 91 (23) (2007) 231922.
- [19] A. Debernardi, S. Baroni, E. Molinari, Phys. Rev. Lett. 75 (9) (1995) 1819–1822.
- [20] G. Deinzer, G. Birner, D. Strauch, Phys. Rev. B 67 (14) (2003) 144304.
- [21] G.P. Srivastava, Physics of Phonons, Taylor and Francis Group, New York, 1990.
 [22] P. Giannozzi, S. Baroni, N. Bonini, M. Calandra, R. Car, C. Cavazzoni, D. Ceresoli,
- G.L. Chiarotti, M. Cococcioni, I. Dabo, A. Dal Corso, S. de Gironcoli, S. Fabris, G. Fratesi, R. Gebauer, U. Gerstmann, C. Gougoussis, A. Kokalj, M. Lazzeri, L. Martin-Samos, N. Marzari, F. Mauri, R. Mazzarello, S. Paolini, A. Pasquarello,
 - L. Paulatto, C. Sbraccia, S. Scandolo, G. Sclauzero, A.P. Seitsonen, A. Smogunov, P. Umari, R.M. Wentzcovitch, J. Phys. Condens. Matter 21 (39) (2009) 395502.
- [23] H.J. Monkhorst, J.D. Pack, Phys. Rev. B 13 (12) (1976) 5188-5192.
- [24] M.G. Holland, Phys. Rev. 134 (2A) (1964) A471-A480.
- [25] M. Clavel, P. Goley, N. Jain, Y. Zhu, M.K. Hudait, IEEE Journal of the Electron Devices Society 3 (3) (2015) 184–193.